Scientific Research Publishing

World Journal of Mechanics, 2018, 8, 137-160
http://www.scirp.org/journal/wjm
ISSN Online: 2160-0503
ISSN Print: 2160-049X

Unsteady MHD Mixed Convection Flow with Slip of a Nanofluid in the Stagnation Region of an Impulsively Rotating Sphere with Effects of Thermal Radiation and Convective Boundary Conditions

Sameh E. Ahmed[1*], Z. Z. Rashed[2]

[1]Mathematics Department, Faculty of Science, South Valley University, Qena, Egypt
[2]Mathematics Department, Faculty of Science and Arts, Jouf University, Qurayyat, KSA
Email: *sameh.hassan@sci.svu.edu.eg

How to cite this paper: Ahmed, S.E. and Rashed, Z.Z. (2018) Unsteady MHD Mixed Convection Flow with Slip of a Nanofluid in the Stagnation Region of an Impulsively Rotating Sphere with Effects of Thermal Radiation and Convective Boundary Conditions. *World Journal of Mechanics*, **8**, 137-160.
https://doi.org/10.4236/wjm.2018.85011

Received: March 30, 2018
Accepted: May 6, 2018
Published: May 9, 2018

Abstract

Unsteady magnetohydrodynamic mixed convection flow of an electrically conducting nanofluid in a stagnation region of a rotating sphere is studied numerically in the present article. Slip and convective boundary conditions are imposed to surface of the sphere and the thermal radiation effects are taken into account. The nanofluid is simulated using Buongiorno's nanofluid model and the nanofluid particle fraction on the boundary is considered to be passively rather than actively controlled. Non-similar solutions are applied on the governing equations and the MATLAB function bvp4c is used to solve the resulting system. Effects of the key-parameters such as slip parameter, Biot number, radiation parameter, rotation parameter, Lewis number and Brownian motion parameter on the fluid flow, temperature and nanoparticle volume fraction characteristics are examined. Details of the numerical solution and a comprehensive discussion with the physical meaning for the obtained results are performed. The results indicated that the increase in slip parameter enhances the velocity profiles, while it decreases the temperature distributions. Also, the increase in either slip parameter or Biot number causes an improvement in the rate of heat transfer.

Keywords

MHD, Slip, Nanofluids, Convective Condition, Radiation

1. Introduction

Nanofluids are new types of fluids consist of a base fluid and suspended nanoparticles (1 - 100 nm). These fluids have a higher thermal conductivity and a single-phase heat transfer coefficient compared with their base fluids [1]. Buongiorno [2] made a test for seven slip mechanisms to determine which of them can produce a relative velocity between the base fluid and nanoparticles. These effects are gravity, fluid drainage, Magnus effect, diffusiophoresis, inertia Brownian diffusion and thermophoresis. His results indicated that only Brownian diffusion and thermophoresis are important in nanofluids. Taken into account this observation, he suggests a model for nanofluids consist of a two-component four-equations nonhomogeneous model for momentum, mass and heat transport. Also, he attributed this abnormal improvement in heat transfer coefficient to the significantly variations of nanofluid properties within the boundary layer due to the effects of thermophoresis and temperature gradient. This mentioned effects can produce a reduction in the fluid viscosity and consequently the heat transfer increases. Kuznetsov and Nield [3] applied the Buongiorno's model [2] to discuss the Pohlhausen, Kuiken and Bejan [4] [5] [6] [7] problems. In this investigation, they assumed that the boundary conditions for the nanoparticle volume fraction are similar to the boundary conditions for the temperature. Kuznetsov and Nield [8] revised their problem [3] to be the nanoparticle volume fraction on the boundary which is passively rather than actively controlled. Makinde and Aziz [9] examined the influence of convective boundary conditions on the convective boundary layer flow of a nanofluid past a stretching sheet. They found that the local concentration of nanoparticles is enhanced as the Biot number increases but decreases as the Lewis number increases. Vajraveu *et al.* [10] analyzed the convective heat transfer and fluid flow over a stretching surface using nanofluids. It is found that the presence of nanoparticles leads to an improvement in the skin friction coefficient. More recently, Ahmed *et al.* [11] discussed the entropy generation analysis due to convective flow of nanofluids over a stretching cylinder. They observed that the increase in suction parameter causes an increase in the entropy generation near the surface. Aly and Ahmed [12] performed an investigation for double diffusive boundary layer flow of a nanofluid over a vertical cylinder. It is found that the local skin friction and the local Sherwood number are enhanced as the buoyancy ratio increases but the local Nusselt number takes the inverse behavior. The convective boundary layer flow of nanofluids over a flat plate under the influence of Newtonian heating and viscous dissipation was presented by Makinde [13]. His results indicated that the increase in nanoparticle volume fraction and Biot number enhances the heat transfer rate. Ahmed and Mahdy [14] studied the magnetohydrodynamic bio-convective flow of nanofluids over a vertical wavy surface. They observed that the increase in either Grashof number or magnetic field parameter results in a reduction in the local Nusselt and Sherwood numbers.

On the other hand, the study of convective boundary layer flow over rotating

bodies of revolution has several engineering applications such as fiber coating, design of rotating machinery, re-entry missile, projectile motion etc. [15]. Because of this importance, many researchers were interest with this subject [16]-[22]. Chamkha and Ahmed [16] reported on MHD double diffusive mixed convection flow in a forward stagnation region of a rotating sphere under the effect of uniform chemical reaction and heat generation. They observed that regardless the cases of CWT and CHMF, the velocity component in the x-direction is enhanced as the acceleration parameter increases. Chamkha and Ahmed [17] studied the unsteady MHD double diffusive boundary layer flow near the stagnation point over a 3D porous body. They observed that the increase in either transpiration parameter or ratio of velocity gradient parameter improves the local Nusselt number. In Chamkha and Ahmed [18], the mixed convection boundary layer flow in the forward stagnation region of a rotating sphere was investigated. The results indicated that the increase in chemical reaction parameter causes an enhancement in the local shear stress and Sherwood number. Faltas and Saad [19] examined the slip effect on Stokes flow between eccentric rotating sphere. They concluded that the effect of slip on the couple is valuable and should not be ignored. Chamkha and Ahmed [20] used the similarity solutions to discuss the unsteady MHD boundary layer flow in a stagnation region of a 3D porous body in the presence of chemical reaction and heat generation/absorption effects. They noted that the increase in either the heat generation/absorption parameter or chemical reaction decreases the local Nusselt number. In [21], the similarity solution was applied on unsteady boundary layer flow over a rotating sphere with a stagnation point. They concluded that the heat transfer obtained by CHF (constant heat flux) case is higher than the case of CWT (constant wall temperature). Takhar and Nath [22] applied a self-similar solution on the unsteady MHD flow over a rotating sphere with a stagnation point region. They showed that the surface shear stress in the x-direction vanishes at a certain value of the acceleration parameter, while the shear stress in the y-direction remains finite.

Ahmed and Mahdy [23] discussed the unsteady magnetohydrodynamic, heat and mass transfer over a rotating sphere with a stagnation point region in the presence of radiation effect. They found that the velocity profiles in x-direction increases as the buoyancy parameter increases. However, they neglected the case of nanofluids and the effects of slip and convective boundary conditions. So, this paper aims to generalize Ahmed and Mahdy [23] using Buongiorno's model [2]. Effects of the slip and convective boundary conditions are taken into account in this study. Non-similar solutions and MATLAB function bvp4c are used to solve the governing equations. Comprehensive discussion with the physical meaning of the findings is performed. To best knowledge of the authors, this problem did not consider before.

2. Problem Formulation

Figure 1 displays the physical model for the unsteady magnetohydrodynamic

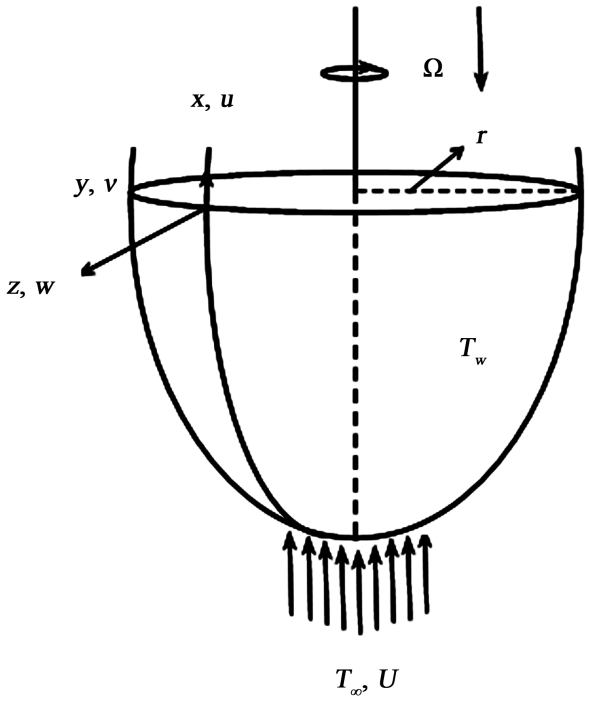

Figure 1. Physical model of the problem.

flow of an incompressible, laminar nanofluid over a rotating sphere with a constant angular velocity Ω in the stagnation region. It is assumed that there is a uniform magnetic field with strength B in the flow domain. A two-phase model (Buongiorno's nanofluid model) is considered to simulate the nanofluid. The ambient velocity, temperature and nanoparticles volume fraction are denoted by $U(x), T_\infty$ and ϕ_∞, respectively, while the noral fluxes of the nanoparticles vanish at the surface of the sphere. Also, a uniform slip and convective boundary conditions are imposed to the wall of the sphere. The thermal radiation is taken into account, but the Joule heating and viscous dissipation effects are neglected. All the fluid properties are constant except the nanofluid density which is approximated using a well-known Boussinesq approximation. Under all these assumptions, the continuity, *x*-component momentum, *y*-component momentum, energy and nanoparticles volume fractions equations are expressed as:

$$\frac{\partial(xu)}{\partial x}+\frac{\partial(xw)}{\partial z}=0 \tag{1}$$

$$\begin{aligned}&\frac{\partial u}{\partial t}+u\frac{\partial u}{\partial x}+w\frac{\partial u}{\partial z}-\frac{v^2}{x}\\&=U\frac{\partial U}{\partial x}+\nu\frac{\partial^2 u}{\partial z^2}+\left[(1-\phi_\infty)\rho_{f\infty}\beta_T(T-T_\infty)\right.\\&\left.-(\rho_P-\rho_{f\infty})(\phi-\phi_\infty)\right]\frac{gx}{r}-\frac{\sigma B_0^2}{\rho_{f\infty}}(u-U)\end{aligned} \tag{2}$$

$$\frac{\partial v}{\partial t}+u\frac{\partial v}{\partial x}+w\frac{\partial v}{\partial z}+\frac{uv}{x}=\nu\frac{\partial^2 v}{\partial z^2}-\frac{\sigma B_0^2}{\rho_f}v \tag{3}$$

$$\frac{\partial T}{\partial t}+u\frac{\partial T}{\partial x}+w\frac{\partial T}{\partial z}$$
$$=\frac{\kappa}{(\rho c)_f}\frac{\partial^2 T}{\partial z^2}+\frac{(\rho c)_P}{(\rho c)_f}\left[D_B\left(\frac{\partial \phi}{\partial z}\frac{\partial T}{\partial z}\right)+\frac{D_T}{T_\infty}\left(\frac{\partial T}{\partial z}\right)^2\right]-\frac{1}{(\rho c)_f}\frac{\partial q}{\partial z} \quad (4)$$

$$\frac{\partial \phi}{\partial t}+u\frac{\partial \phi}{\partial x}+w\frac{\partial \phi}{\partial z}=D_B\frac{\partial^2 \phi}{\partial z^2}+\frac{D_T}{T_\infty}\frac{\partial^2 T}{\partial z^2} \quad (5)$$

In Equations (1)-(4), u, v and w are the velocity components in x, y and z-direction, respectively, ϕ is the nanoparticle volume fraction, ρ is the density, ν is the kinematic viscosity, T is the temperature, β_T is the thermal expansion, g is the gravity acceleration, σ is the electrical conductivity, B_0 is the magnetic strength, k is the thermal conductivity, D_B is Brownian diffusion coefficient, D_T is thermophoretic diffusion, C is the specific heat, q is the radiative heat flux and the subscripts f, p and ∞ refer to base fluid, nanoparticle and free stream condition, respectively.

The radiative flux q can be expressed using the Rossel and approximation [24] as:

$$q=\frac{-4\sigma_1}{3k^*}\frac{\partial T^4}{\partial z} \quad (6)$$

where, σ_1 is the Stefan-Boltzmann constant and k^* is the absorption coefficient. Expanding T^4 using Taylor series about T_∞ and neglecting the higher terms, we obtain:

$$T^4=-3T_\infty^4+4T_\infty^3 T \quad (7)$$

Substituting Equations (6) and (7) in Equation (4), we get:

$$\frac{\partial T}{\partial t}+u\frac{\partial T}{\partial x}+w\frac{\partial T}{\partial z}$$
$$=\left(\frac{\kappa}{(\rho c)_f}+\frac{16T_\infty^3\sigma_1}{3k^*(\rho c)_f}\right)\frac{\partial^2 T}{\partial z^2}+\frac{(\rho c)_P}{(\rho c)_f}\left[D_B\left(\frac{\partial \phi}{\partial z}\frac{\partial T}{\partial z}\right)+\frac{D_T}{T_\infty}\left(\frac{\partial T}{\partial z}\right)^2\right] \quad (8)$$

The corresponding initial and boundary conditions are:

$$t<0, u(x,z,t)=v(x,z,t)=w(x,z,t)=0, T(x,z,t)=T_\infty, \phi(x,z,t)=\phi_\infty \quad (9a)$$

$$t\geq 0, u(x,0,t)=N\mu\frac{\partial u}{\partial z}, v(x,0,t)=\Omega x, w(x,0,t)=0,$$
$$k\frac{\partial T}{\partial z}=h_f\left(T-T_f\right), D_B\frac{\partial \phi(x,0,t)}{\partial z}+\frac{D_T}{T_\infty}\frac{\partial T(x,0,t)}{\partial z}=0 \quad (9b)$$

$$t\geq 0, u(x,\infty,t)=U(x), v(x,\infty,t)=0, T(x,\infty,t)=T_\infty,$$
$$C(x,\infty,t)=C_\infty, \phi(x,\infty,t)=\varphi_\infty \quad (9c)$$

where, is the dimensional slip parameter, μ is the dynamic viscosity, Ω is the angular velocity of the sphere and h_f is the convective heat transfer.

Introducing the following dimensionless variables:

$$\xi = 1-\exp(-at),\ \eta = \left(\frac{2a}{\nu}\right)^{\frac{1}{2}} \xi^{-\frac{1}{2}} z,\ a>0, U = ax,$$

$$v(x,z,t) = \Omega S(\xi,\eta),\ w(x,z,t) = -(2a\nu)^{\frac{1}{2}} \xi^{\frac{1}{2}} F(\xi,\eta), \tag{10}$$

$$\lambda = \left(\frac{\Omega}{a}\right)^2,\ \frac{T(x,z,t)-T_\infty}{T_f - T_\infty} = \theta(\xi,\eta),\ \frac{\phi(x,z,t)-\phi_\infty}{\phi_\infty} = \varphi(\xi,\eta)$$

Substituting Equation (10) into Equations (2), (3), (5) and (8), the following non-similar equations are obtained:

$$F''' + \xi FF'' + \frac{1}{4}\eta(1-\xi)F'' + \frac{1}{2}\xi\left(1-F'^2+\lambda S^2\right) + \frac{1}{2}M\xi(1-F') + \frac{1}{2}\xi\gamma(\theta - N_r\varphi) = \frac{1}{2}\xi(1-\xi)\frac{\partial F'}{\partial \xi} \tag{11}$$

$$S'' + \xi(S'F - F'S) + \frac{1}{4}\eta(1-\xi)S' - \frac{1}{2}M\xi S = \frac{1}{2}\xi(1-\xi)\frac{\partial S}{\partial \xi} \tag{12}$$

$$\frac{1}{Pr}\left(1+\frac{4}{3R}\right)\theta'' + \frac{1}{4}\eta(1-\xi)\theta' + \xi F\theta' + + N_b\varphi'\theta' + N_T\theta'^2 = \frac{1}{2}\xi(1-\xi)\frac{\partial \theta}{\partial \xi} \tag{13}$$

$$\varphi'' + \frac{N_T}{N_b}\theta'' + Le\xi F\varphi' + \frac{Le}{4}(1-\xi)\eta\varphi' = \frac{Le}{2}\xi(1-\xi)\frac{\partial \varphi}{\partial \xi} \tag{14}$$

where, $Gr_R = \dfrac{g\beta_T(T_f - T_\infty)(1-\phi_\infty)\rho_{f\infty} r^3}{\nu^2}$ is the Grashof number, $\gamma = \dfrac{Gr_R}{Re_R^2}$ is the buoyancy parameter, $Re_R = \dfrac{r^2 a}{\nu}$ is the Reynolds number, $M = \dfrac{\sigma B_0^2}{a\rho_{f\infty}}$ is the magnetic field parameter , $N_r = \dfrac{(\rho_p - \rho_{f\infty})\phi_\infty}{(1-\phi_\infty)\rho_{f\infty}(T_f - T_\infty)\beta_T}$ is the buoyancy ratio, $\lambda = \left(\dfrac{\Omega}{a}\right)^2$ is the rotation parameter, $N_b = \dfrac{(\rho c)_p D_B \phi_\infty}{(\rho c)_f \nu}$ is the Brownian motion parameter, $N_t = \dfrac{(\rho c)_p D_T (T_f - T_\infty)}{(\rho c)_f T_\infty \nu}$ is the thermophoreses parameter, $Pr = \dfrac{\mu c_p}{k}$ is the Prandtl number, $Le = \dfrac{\nu}{D_B}$ is the Lewis number.

The boundary conditions are converted to:

$$F'(\xi,0) = \delta F''(\xi,0),\ S(\xi,0) = 1,\ F(\xi,0) = 0,$$
$$\theta'(\xi,0) = Bi(\theta(\xi,0)-1),\ N_b\varphi'(\xi,0) + N_t\theta'(\xi,0) = 0$$
$$F'(\xi,\infty) = 1,\ S(\xi,\infty) = 0,\ \theta(\xi,\infty) = 0,\ \varphi(\xi,\infty) = 0 \tag{15}$$

where, $\delta = N\mu\left[\dfrac{2a}{\upsilon\xi}\right]^{\frac{1}{2}}$ is the slip parameter and $Bi = \dfrac{h_f}{k}\left[\dfrac{\nu\xi}{2a}\right]^{\frac{1}{2}}$ is the Biot number.

3. Numerical Solutions

In this section the MATLAB function bvp4c is applied to solve Equations

(11)-(14) with the boundary conditions (15). The first step in this technique is the converting the system (11)-(14) to an ordinary differential equations system, so all the derivatives with respect to ξ in this system are dropped down, thus:

$$\begin{aligned} &F''' + \xi FF'' + \frac{1}{4}\eta(1-\xi)F'' + \frac{1}{2}\xi\left(1-F'^2+\lambda S^2\right) \\ &+\frac{1}{2}M\xi(1-F') + \frac{1}{2}\xi\ \gamma(\theta - N_{rr}\varphi) = 0 \end{aligned} \tag{16}$$

$$S'' + \xi(S'F - F'S) + \frac{1}{4}\eta(1-\xi)S' - \frac{1}{2}M\xi S = 0 \tag{17}$$

$$\frac{1}{Pr}\left(1+\frac{4}{3R}\right)\theta'' + \frac{1}{4}\eta(1-\xi)\theta' + \xi F\theta' + N_b\varphi'\theta' + N_T\theta'^2 = 0 \tag{18}$$

$$\varphi'' + \frac{N_T}{N_b}\theta'' + Le\xi F\varphi' + \frac{Le}{4}(1-\xi)\eta\varphi' = 0 \tag{19}$$

Subject to the boundary conditions:

$$\begin{aligned} &F'(\xi,0) = \delta F''(\xi,0),\ S(\xi,0) = 1,\ F(\xi,0) = 0, \\ &\theta'(\xi,0) = Bi\left(\theta(\xi,0)-1\right),\ N_b\varphi'(\xi,0) + N_t\theta'(\xi,0) = 0 \\ &F'(\xi,\infty) = 1,\ S(\xi,\infty) = 0,\ \theta(\xi,\infty) = 0,\ \varphi(\xi,\infty) = 0 \end{aligned} \tag{20}$$

In the second step, all the neglected terms in previous system are restored and the following new variables are introduced:

$$F_1 = \frac{\partial F}{\partial \xi},\ S_1 = \frac{\partial S}{\partial \xi},\ \theta_1 = \frac{\partial \theta}{\partial \xi} \text{ and } \varphi_1 = \frac{\partial \varphi}{\partial \xi} \tag{21}$$

Thus, the governing equations are:

$$\begin{aligned} &F''' + \xi FF'' + \frac{1}{4}\eta(1-\xi)F'' + \frac{1}{2}\xi\left(1-F'^2+\lambda S^2\right) + \frac{1}{2}M\xi(1-F') \\ &+\frac{1}{2}\xi\gamma(\theta - N_{rr}\varphi) = \frac{1}{2}\xi(1-\xi)F_1' \end{aligned} \tag{22}$$

$$S'' + \xi(S'F - F'S) + \frac{1}{4}\eta(1-\xi)S' - \frac{1}{2}M\xi S = \frac{1}{2}\xi(1-\xi)S_1 \tag{23}$$

$$\frac{1}{Pr}\left(1+\frac{4}{3R}\right)\theta'' + \frac{1}{4}\eta(1-\xi)\theta' + \xi F\theta' + N_b\varphi'\theta' + N_T\theta'^2 = \frac{1}{2}\xi(1-\xi)\theta_1 \tag{24}$$

$$\varphi'' + \frac{N_T}{N_b}\theta'' + Le\xi F\varphi' + \frac{Le}{4}(1-\xi)\eta\varphi' = \frac{Le}{2}\xi(1-\xi)\varphi_1 \tag{25}$$

Subject to the boundary conditions:

$$\begin{aligned} &F'(\xi,0) = \delta F''(\xi,0),\ S(\xi,0) = 1,\ F(\xi,0) = 0, \\ &\theta'(\xi,0) = Bi\left(\theta(\xi,0)-1\right),\ N_b\varphi'(\xi,0) + N_t\theta'(\xi,0) = 0 \\ &F'(\xi,\infty) = 1,\ S(\xi,\infty) = 0,\ \theta(\xi,\infty) = 0,\ \varphi(\xi,\infty) = 0 \end{aligned} \tag{26}$$

There are four additional equations are needed with appropriate boundary conditions to evaluate the four new variables F_1, S_1, θ_1 and φ_1. These can be obtained by differentiating Equations (22)-(26) with respect to ξ and neglecting

the terms $\frac{\partial F_1}{\partial \xi}, \frac{\partial S_1}{\partial \xi}, \frac{\partial \theta_1}{\partial \xi}$ and $\frac{\partial \varphi_1}{\partial \xi}$, it can be obtained:

$$\begin{aligned} &F_1''' + FF'' + \xi\left(F_1F'' + FF_1''\right) + \frac{1}{4}\eta\left(1-\xi\right)F_1'' - \frac{1}{4}\eta F'' \\ &+\frac{1}{2}\left(1-F'^2 + \lambda S^2 + \xi\left(-2F'F_1' + 2\lambda SS_1\right)\right) + \frac{1}{2}M\left(1-F'\right) - \frac{1}{2}M\xi F_1' \\ &+\frac{1}{2}\gamma\left(\theta - N_{rr}\varphi\right) + \frac{1}{2}\xi\ \gamma\left(\theta_1 - N_{rr}\varphi_1\right) = \frac{1}{2}\left(1-\xi\right)F_1' - \frac{1}{2}\xi F_1' \end{aligned} \tag{27}$$

$$\begin{aligned} &S_1'' + \left(S'F - F'S\right) + \xi\left(S_1'F + S'F_1 - F_1'S - F'S_1\right) - \frac{1}{4}\eta S' + \frac{1}{4}\eta\left(1-\xi\right)S_1' \\ &-\frac{1}{2}M\left(\xi S_1 + S\right) = \frac{1}{2}\left(1-\xi\right)S_1 - \frac{1}{2}\xi S_1 \end{aligned} \tag{28}$$

$$\begin{aligned} &\frac{1}{Pr}\left(1+\frac{4}{3R}\right)\theta_1'' - \frac{1}{4}\eta\theta' + \frac{1}{4}\eta\left(1-\xi\right)\theta_1' + F\theta' + \xi\left(F_1\theta' + F\theta_1'\right) \\ &+N_b\left(\varphi_1'\theta' + \varphi'\theta_1'\right) + 2N_T\theta'\theta_1' = \frac{1}{2}\left(1-\xi\right)\theta_1 - \frac{1}{2}\xi\theta_1 \end{aligned} \tag{29}$$

$$\begin{aligned} &\varphi_1'' + \frac{N_T}{N_b}\theta_1'' + LeF\varphi' + Le\ \xi\left(F_1\varphi' + F\varphi_1'\right) - \frac{Le}{4}\eta\varphi' + \frac{Le}{4}\left(1-\xi\right)\eta\varphi_1' \\ &= \frac{Le}{2}\left(1-\xi\right)\varphi_1 - \frac{Le}{2}\xi\varphi_1 \end{aligned} \tag{30}$$

Subjected to the boundary conditions:

$$\begin{aligned} &F_1'\left(\xi,0\right) = \delta F_1''\left(\xi,0\right),\ S_1\left(\xi,0\right) = 0,\ F_1\left(\xi,0\right) = 0, \\ &\theta_1'\left(\xi,0\right) = Bi\theta_1\left(\xi,0\right),\ N_b\varphi_1'\left(\xi,0\right) + N_t\theta_1'\left(\xi,0\right) = 0 \\ &F_1'\left(\xi,\infty\right) = 0,\ S_1\left(\xi,\infty\right) = 0,\ \theta_1\left(\xi,\infty\right) = 0,\ \varphi_1\left(\xi,\infty\right) = 0 \end{aligned} \tag{31}$$

Equations (16)-(19), with the boundary conditions (20) and Equations (27)-(30) with the boundary conditions (31) are solved numerically using MATLAB software. The value of $\eta_{\max}$ is set to be equal 10 and the step size is $\Delta\eta = 0.02$. This method is found to be suitable and gives results those are very close to Ahmed and Mahdy [23]. As it can be noted from **Figure 2**, the present method compares very well with Ahmed and Mahdy [23].

4. Results and Discussion

Figure 3 and **Figure 4** display effects of the slip parameter δ on the dimensionless velocity in the x-direction and temperature. The results indicated that the velocity value increases as the slip parameter increases but the temperature distributions decreases hence the thickness of the thermal boundary layer increases. Physically, the increase in slip parameters causes an enhancement in the velocity gradients on the sphere surface which in turn increases the fluid activity, rate of heat transfer and decreases the temperature as well.

Figure 5 shows that the nanoparticle volume fraction profiles increase with increasing δ near the rotating sphere surface up to a certain value of η but beyond this point, the opposite trend is observed. In **Figures 6-8**, the influence of thermophoresis parameter Nt on the velocity in the x-direction, temperature

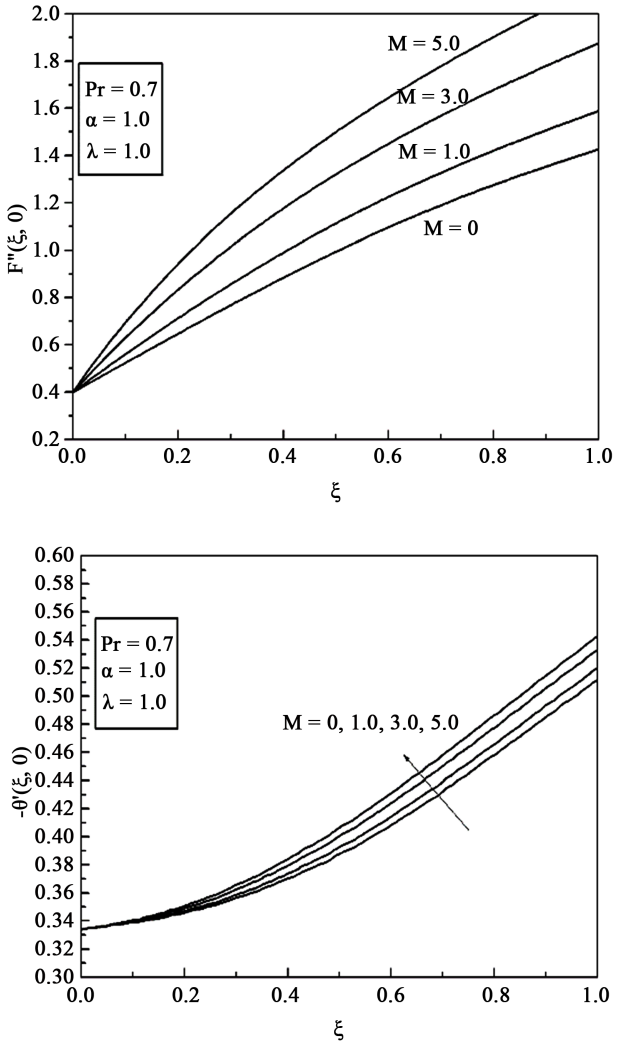

Figure 2. Comparison of the present results and those obtained by Ahmed and Mahdy [23].

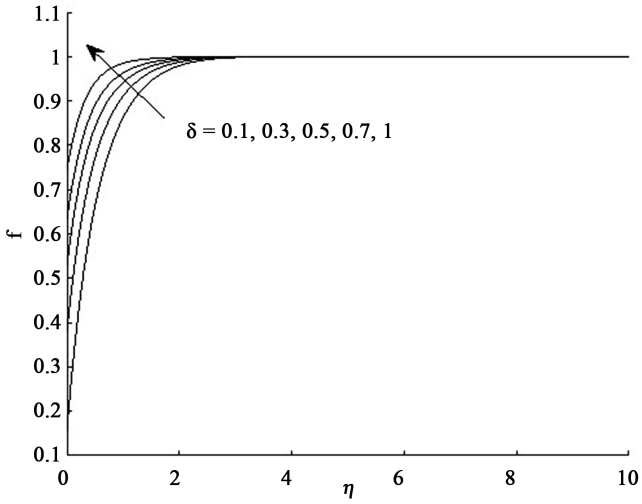

Figure 3. Profiles of the velocity in the x-direction for different values of δ at $Bi = 0.5$, $M = 5$, $R = 5$, $Le = 10$, $Pr = 10$, $Nt = Nb = Nr = 0.5$, $\gamma = \lambda = 5$, $\xi = 0.5$.

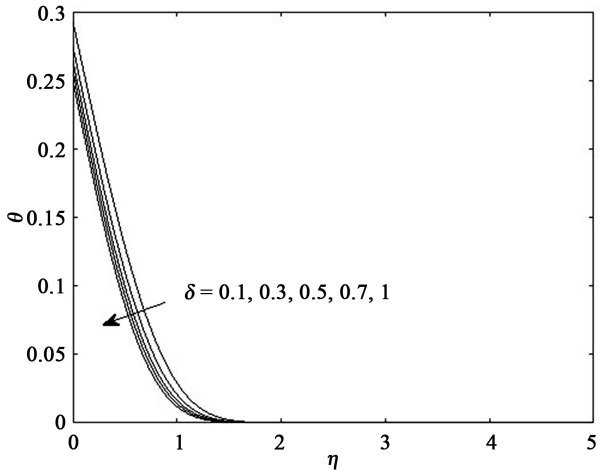

Figure 4. Temperature distributions for different values of δ at $Bi = 0.5$, $M = 5$, $R = 5$, $Le = 10$, $Pr = 10$, $Nt = Nb = Nr = 0.5$, $\gamma = \lambda = 5$, $\xi = 0.5$.

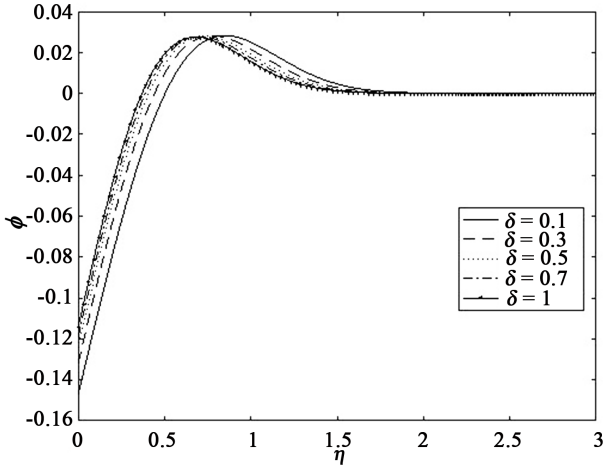

Figure 5. Profiles of the nanoparticle volume fraction for different values of δ at $Bi = 0.5$, $M = 5$, $R = 5$, $Le = 10$, $Pr = 10$, $Nt = Nb = Nr = 0.5$, $\gamma = \lambda = 5$, $\xi = 0.5$.

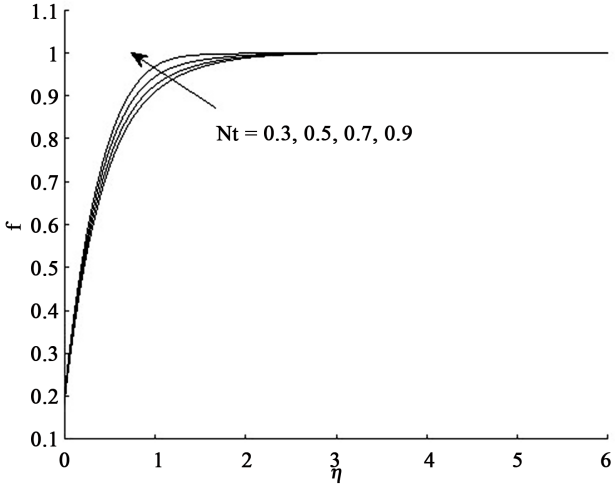

Figure 6. Profiles of the velocity in the x-direction for different values of Nt at $Bi = 10$, $M = 5$, $R = 5$, $Le = 10$, $Pr = 10$, $Nb = Nr = 0.5$, $\delta = 0.1$, $\gamma = \lambda = 5$, $\xi = 0.5$.

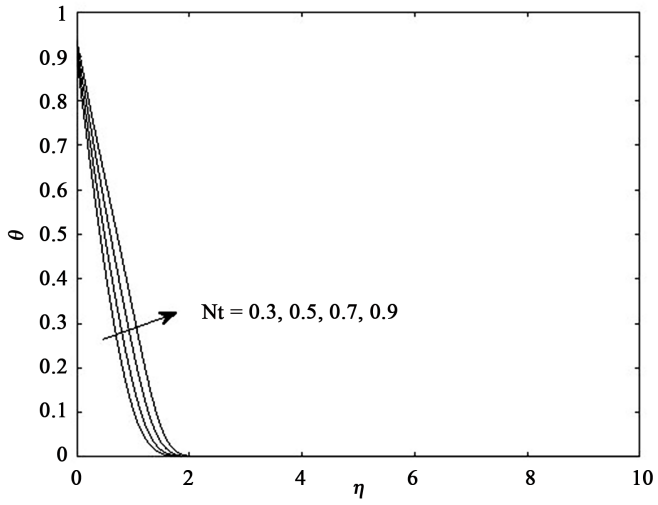

Figure 7. Temperature distributions for different values of Nt at $Bi = 10$, $M = 5$, $R = 5$, $Le = 10$, $Pr = 10$, $Nb = Nr = 0.5$, $\delta = 0.1$, $\gamma = \lambda = 5$, $\xi = 0.5$.

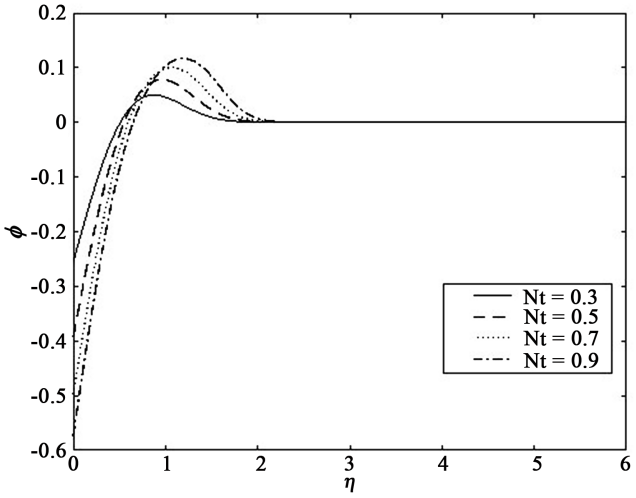

Figure 8. Profiles of the nanoparticle volume fraction for different values of Nt at $Bi = 10$, $M = 5$, $R = 5$, $Le = 10$, $Pr = 10$, $Nb = Nr = 0.5$,$\delta = 0.1$, $\gamma = \lambda = 5$, $\xi = 0.5$.

and nanoparticle volume fraction profiles are illustrated. It is found that, the increase in Nt leads to an increase in the velocity profiles and temperature distributions but the nanoparticle volume fraction profiles decrease with the increase in δ near the sphere surface, whereas at $\eta > 1$, the inverse behavior is observed. Also, the thermal boundary layer increases, slightly, along with the increase in Nt. In Figures 9-11, the effects of Biot number Bi on the velocity profiles in the x-direction, temperature distribution and the nanoparticle volume fraction profiles are presented. It can be noted that the increase in Bi enhances the velocity profiles and temperature distributions, while on contrary the profiles of nanoparticle volume fraction are reduced. Additionally, this mentioned behavior of ϕ is noted near the surface but far away from the sphere surface, the increase in Bi improves the distributions of ϕ. Here, it should be mentioned that when $Bi \to \infty$, the constant wall temperature case (CWT) is obtained. From the

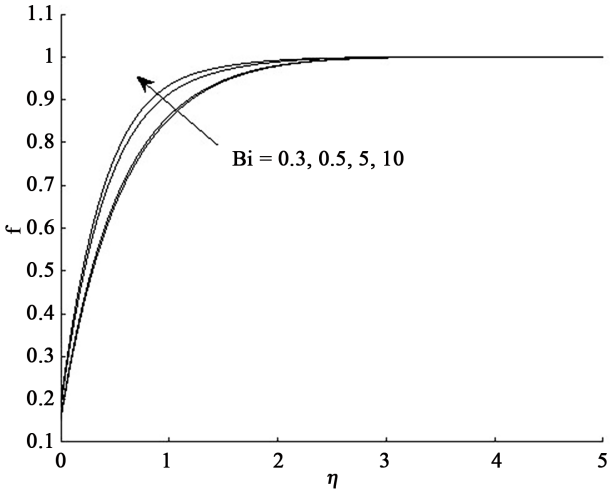

Figure 9. Profiles the velocity in x-direction for different values of Bi at $M = 5$, $R = 5$, $Le = 10$, $Pr = 10$, $Nt = Nb = Nr = 0.5$, $\delta = 0.1$, $\gamma = \lambda = 5$, $\xi = 0.5$.

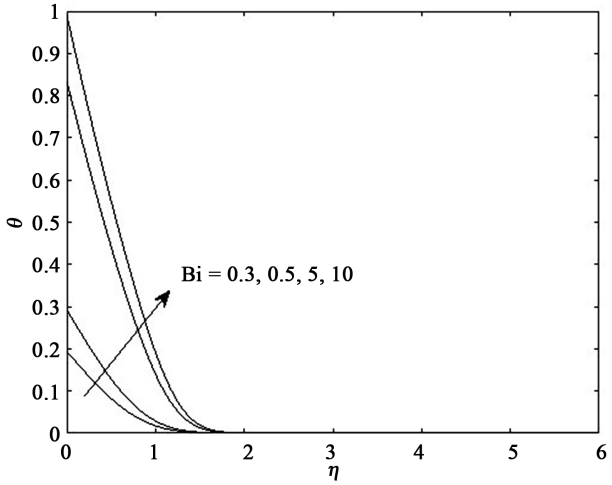

Figure 10. Temperature distributions for different values of Bi at $M = 5$, $R = 5$, $Le = 10$, $Pr = 10$, $Nt = Nb = Nr = 0.5$, $\delta = 0.1$, $\gamma = \lambda = 5$, $\xi = 0.5$.

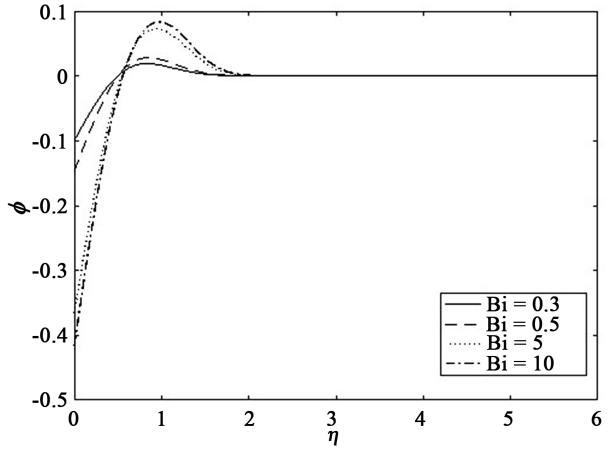

Figure 11. Profiles of the nanoparticle volume fraction for different values of Bi at $M = 5$, $R = 5$, $Le = 10$, $Pr = 10$, $Nt = Nb = Nr = 0.5$, $\delta = 0.1$, $\gamma = \lambda = 5$, $\xi = 0.5$.

physical view, the increase in Bi enhances the temperature differences at the wall which in turn augments the mixed convection and consequently increases the velocity temperature distributions.

Figures 12-14 display effect of the radiation parameter R on the velocity in the x-direction, temperature and the nanoparticle volume fraction profiles. It is found that the increase in R leads to a reduction in the velocity and temperature profiles. Further, the nanoparticle volume fraction profiles decrease with increasing R near the surface up to a certain value of η but beyond this point, the opposite tendency is observed.

The effect of variations of Lewis Le on the velocity profiles in the x-direction for different values of slip parameter δ is examined with the help of Figure 15. It is found that the increase in Le resists the fluid flow in this direction regardless of the value of δ. This can be attributed to the velocity boundary layer thickness which increases as Le increases and therefore the velocity profiles decrease.

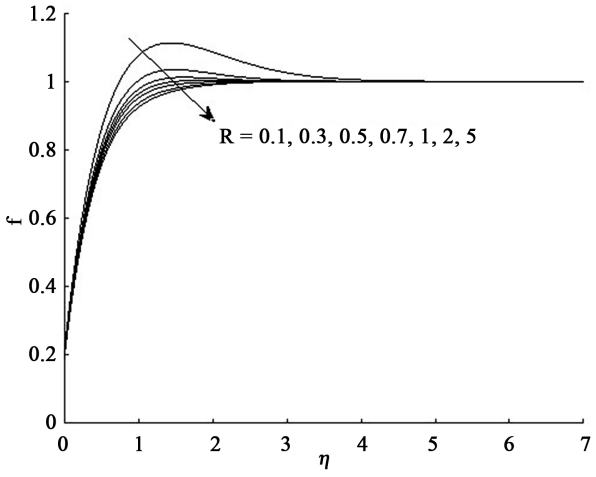

Figure 12. Profiles of the velocity in x-directions for different values of R at Bi = 10, M = 5, Le = 10, Pr = 10, Nt = Nb = Nr = 0.5, δ = 0.1, γ = λ = 5, ξ = 0.5.

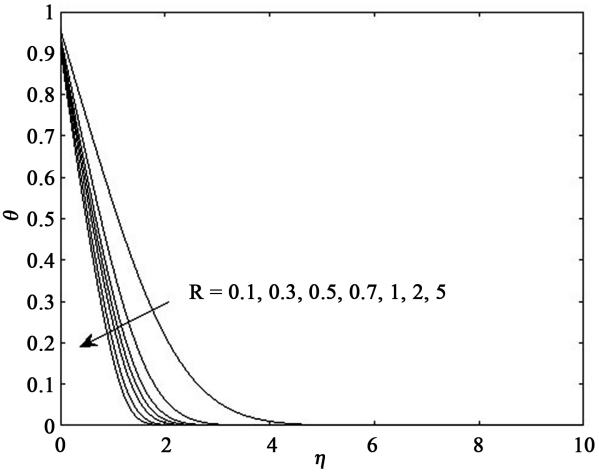

Figure 13. Temperature distributions for different values of R at Bi = 10, M = 5, Le = 10, Pr = 10, Nt = Nb = Nr = 0.5, δ = 0.1, γ = λ = 5, ξ = 0.5.

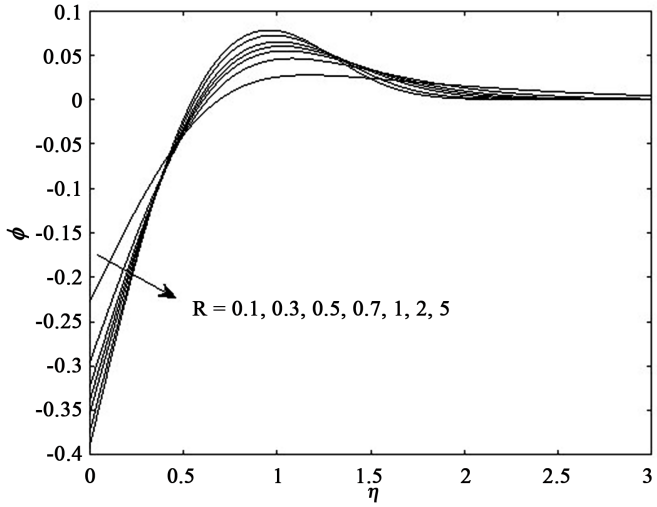

Figure 14. Profiles of the nanoparticle volume fraction for different values of R at $Bi = 10$, $M = 5$, $Le = 10$, $Pr = 10$, $Nt = Nb = Nr = 0.5$, $\delta = 0.1$, $\gamma = \lambda = 5$, $\xi = 0.5$.

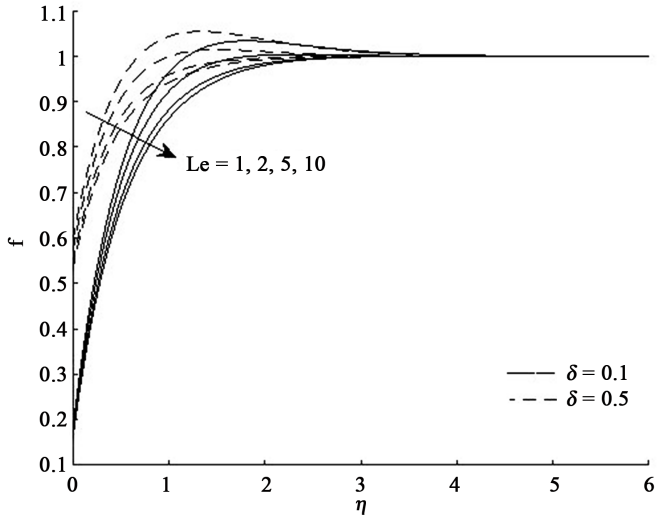

Figure 15. Profiles of the velocity in the x-direction for different values of Le and δ at at $Bi = 0.5$, $M = 5$, $R = 5$, $Pr = 10$, $Nt = Nb = Nr = 0.5$, $\gamma = \lambda = 5$, $\xi = 0.5$.

Figure 16 shows that as the Prandtl number Pr increases, the temperature distribution decreases. Here it should be mentioned that if δ^* denoted the velocity boundary layer thickness and δ_T represented the thermal boundary layer thickness, so if $Pr = 1$, then $\delta^* = \delta_T$, if $Pr < 1$ then $\delta^* < \delta_T$ and if $Pr > 1$, then $\delta^* > \delta_T$. Consequently, the thermal boundary layer is inversely proportional with the values of Pr, so the temperature distributions are reduced as Pr increases.

Also, the same effect is observed for the increase in δ, moreover the thickness of the thermal boundary layer decreases. As can be observed in **Figure 17** increasing value of the Pr the nanoparticle volume fraction profiles increase near the stretching sheet wall up to a certain value of η but beyond this point, the opposite trend is observed.

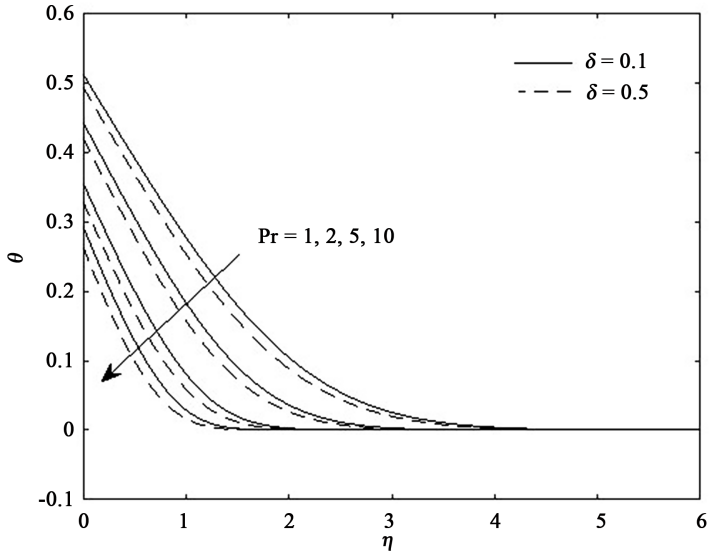

Figure 16. Temperature distributions for different values of Pr and δ at $Bi = 0.5$, $M = 5$, $R = 5$, $Le = 10$, $Nt = Nb = Nr = 0.5$, $\gamma = \lambda = 5$, $\xi = 0.5$.

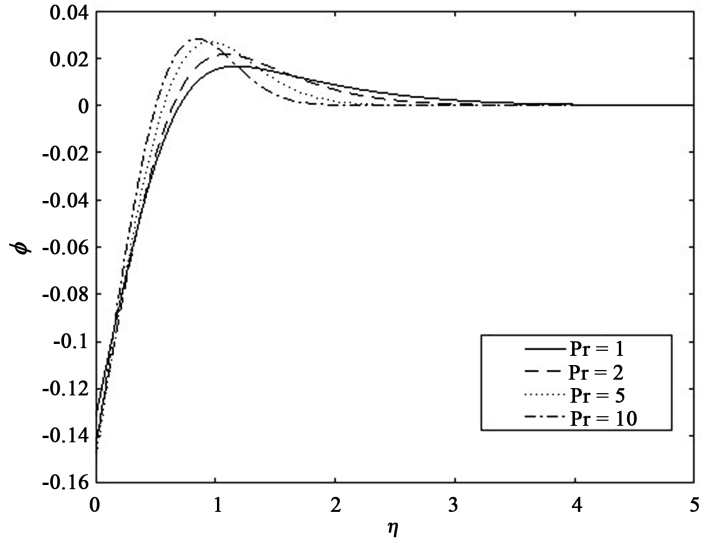

Figure 17. Profiles of the nanoparticle volume fraction for different values of Pr at $Bi = 0.5$, $M = 5$, $R = 5$, $Le = 10$, $Nt = Nb = Nr = 0.5$, $\delta = 0.1$, $\gamma = \lambda = 5$, $\xi = 0.5$.

In **Figure 18** and **Figure 19** respectively shows the effects of the rotation parameter λ and the buoyancy parameter γ on the velocity profiles in the x-direction. It clear increase in λ, γ leads to an increase in the velocity profiles .The physical explanation for this behavior is attributed to the fluid momentum which increases by increase rotation parameter.

The effects of the rotation parameter λ and the slip parameter δ on the local skin friction coefficient $F''(\xi,0)$ are presented in **Figure 20** and **Figure 21**. It is observed from these figures that as the rotation parameter λ increases of $F''(\xi,0)$ increase Also, the same effect is observed for the increase in δ, but at $\delta = 0.2$, ($\xi > 0.6$) the $F''(\xi,0)$ has different behavior.

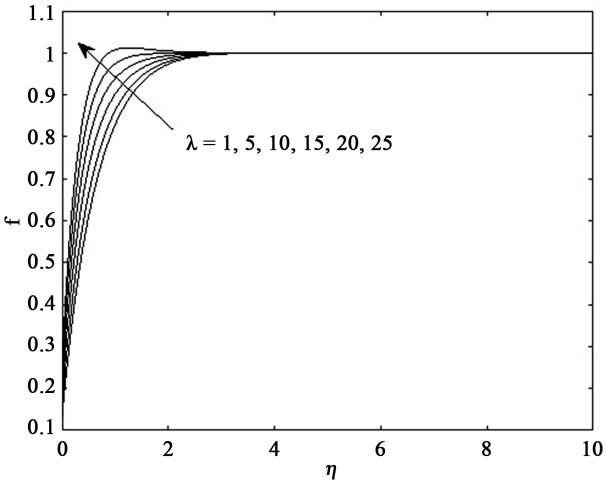

Figure 18. Profiles of the velocity in x-directions for different values of λ at Bi = 0.5, $M = R = 5$, $Le = 10$, $Pr = 10$, $Nt = Nb = Nr = 0.5$, $\delta = 0.1$, $\gamma = \lambda = 5$, $\xi = 0.5$.

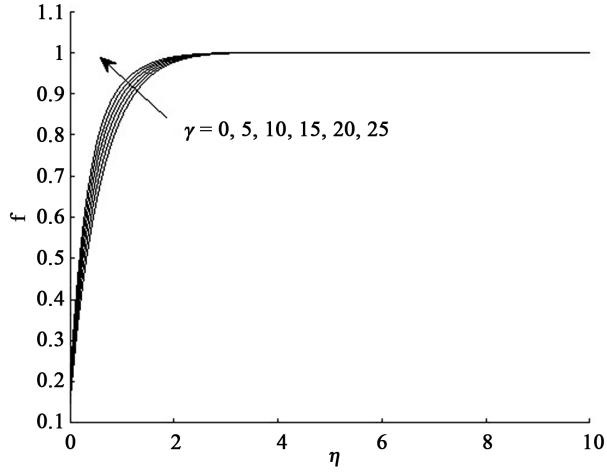

Figure 19. Profiles of the velocity in x-directions for different values of γ at Bi = 0.5, $M = R = 5$, $Le = 10$, $Pr = 10$, $Nt = Nb = Nr = 0.5$, $\delta = 0.1$, $\lambda = 5$, $\xi = 0.5$.

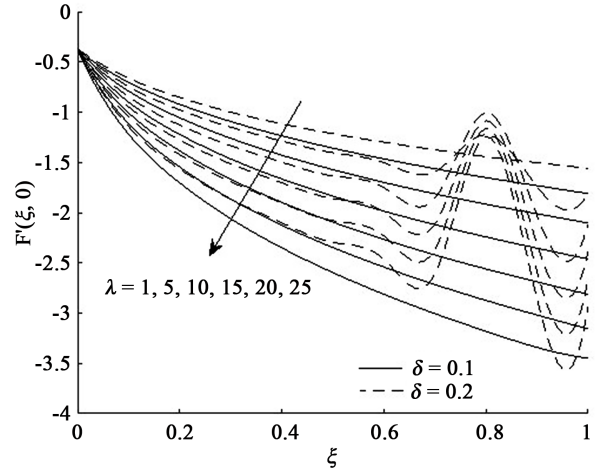

Figure 20. Local skin friction coefficient for different values of λ and δ at Bi = 0.5, $M = 5$, $R = 5$, $Le = 10$, $Pr = 10$, $Nt = Nb = Nr = 0.5$, $\gamma = 5$, $\xi = 0.5$.

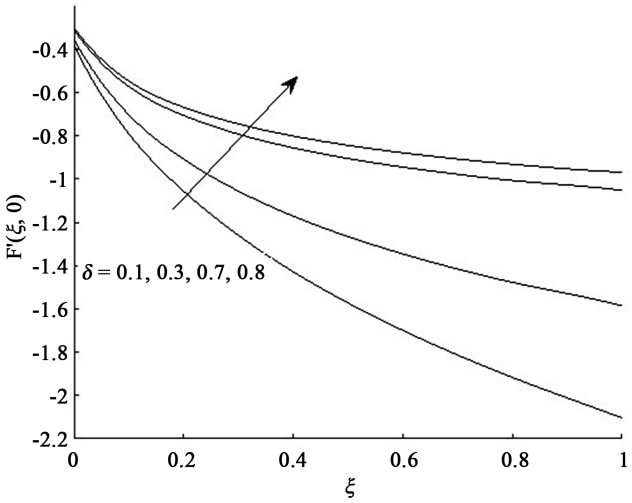

Figure 21. Local skin friction coefficient for different values of δ at $Bi = 0.5$, $M = 5$, $R = 5$, $Le = 10$, $Pr = 10$, $Nt = Nb = Nr = 0.5$, $\gamma = \lambda = 5$, $\xi = 0.5$.

The effects of slip parameter δ on the local Nusselt and Sherwood numbers are shown in **Figures 22** and **Figure 23** respectively. It is seen that the local Nusselt number increases with increasing δ, while local Sherwood number decrease. These behaviors is due to the fact that the increase in slip parameter improves the mixed convection case and thus the rate of heat transfer is enhanced

In **Figure 24** and **Figure 25**, the behavior of local Nusselt number and Sherwood number for various values of Biot number Bi is noted. The results indicate that the increase in Bi number cause an enhancement in the temperature gradients at the surface and consequently the rate of heat transfer is augmented, while the opposite behavior $-\phi'(\xi,0)$. Also thermal boundary layer thickness increases.

Figure 26 shows the influences of Brownian motion parameter Nb on the local Sherwood number $-\phi'(\xi,0)$. It is observed that as the Brownian motion parameter increases of of the local Sherwood number increase. Physically, the increase in Brownian motion parameter increases the net movement of atoms or molecules from the region near the surface where the high concentration of nanoparticle to the region of low concentration of nanoparticle (free stream region) which results in the increase in Sherwood number.

Figure 27 and **Figure 28** exhibit the effect of thermophoresis parameter Nt on the local Nusselt and Sherwood numbers, respectively. It is clear that the increase in Nt leads to a decrease in the local Nusselt and Sherwood numbers.

5. Conclusions

This paper discussed the unsteady MHD mixed convection flow along rotating spheres with a stagnation point in the presence of thermal radiation, slip and convective boundary conditions. The problem was formulated using Navier stokes equations with boundary layer approximations and then solved numerically using MATLAB software. The obtained results were presented in terms of

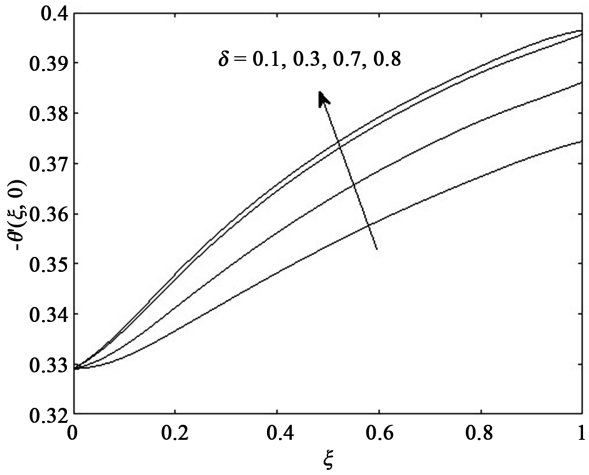

Figure 22. Local Nusselt number for different values of δ at $Bi = 0.5$, $M = 5$, $R = 5$, $Le = 10$, $Pr = 10$, $Nt = Nb = Nr = 0.5$, $\gamma = \lambda = 5$, $\xi = 0.5$.

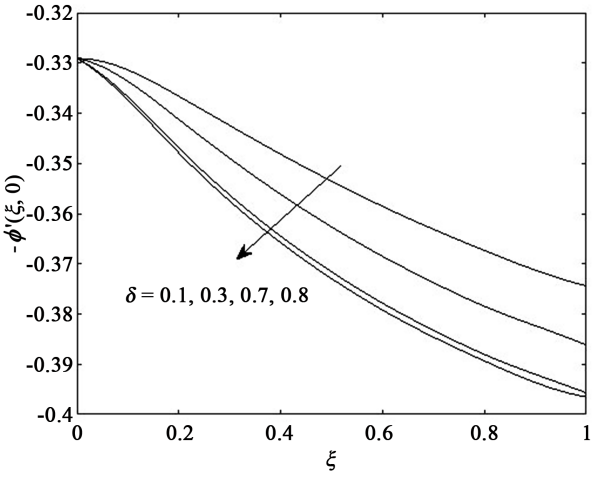

Figure 23. Local Sherwood number for different values of δ at $Bi = 0.5$, $M = 5$, $R = 5$, $Le = 10$, $Pr = 10$, $Nt = Nb = Nr = 0.5$, $\gamma = \lambda = 5$, $\xi = 0.5$.

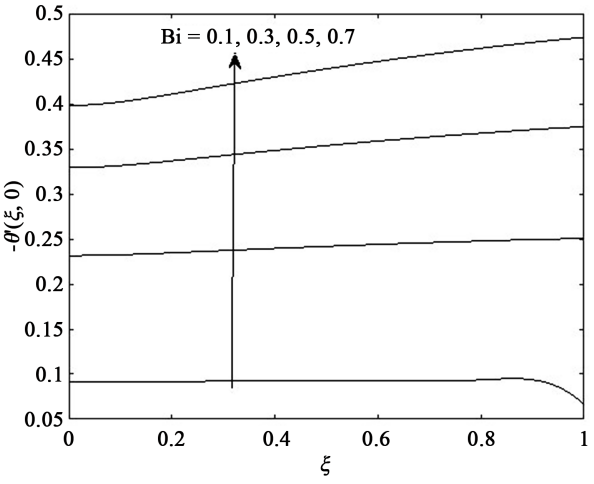

Figure 24. Local Nusselt number for different values of Bi at $M = 5$, $R = 5$, $Le = 10$, $Pr = 10$, $Nt = Nb = Nr = 0.5$, $\delta = 0.1$, $\gamma = \lambda = 5$, $\xi = 0.5$.

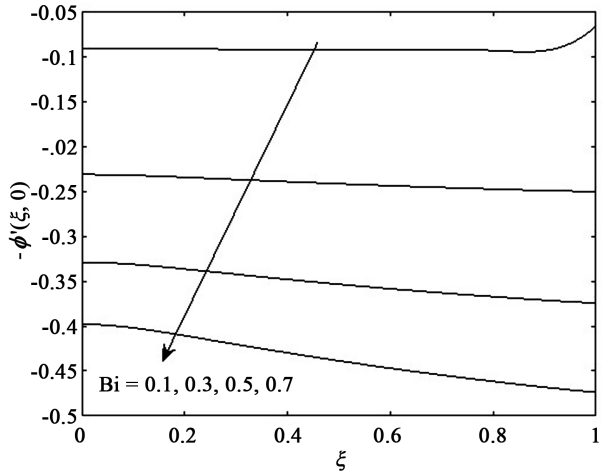

Figure 25. Local Sherwood number for different values of Bi at $M = 5$, $R = 5$, $Le = 10$, Pr = 10, $Nt = Nb = Nr = 0.5$, $\delta = 0.1$, $\gamma = \lambda = 5$, $\xi = 0.5$.

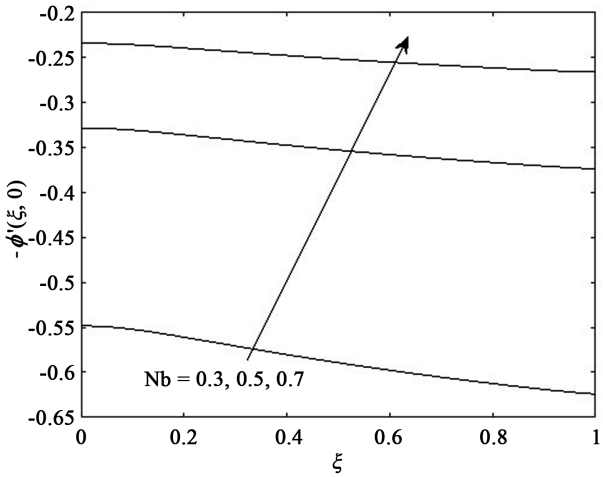

Figure 26. Local Sherwood number for different values of Nb at $Bi = 0.5$, $M = 5$, $R = 5$, $Le = 10$, $Pr = 10$, $Nt = Nr = 0.5$, $\delta = 0.1$, $\gamma = \lambda = 5$, $\xi = 0.5$.

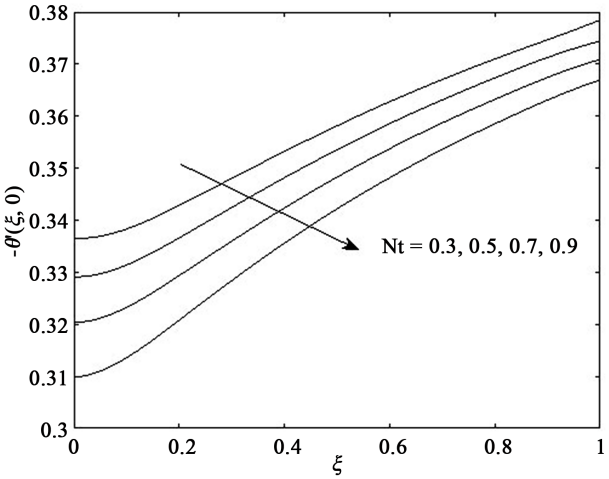

Figure 27. Local Nusselt number for different values of Nt at $Bi = 0.5$, $M = 5$, $R = 5$, $Le = 10$, $Pr = 10$, $Nb = Nr = 0.5$, $\delta = 0.1$, $\gamma = \lambda = 5$, $\xi = 0.5$.

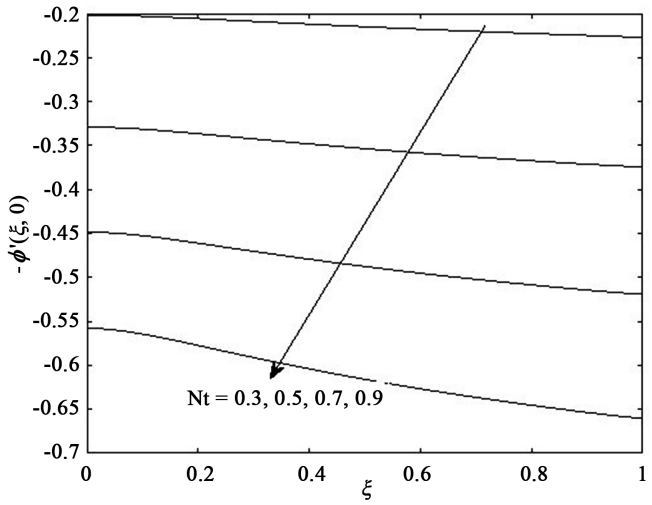

Figure 28. Local Sherwood number for different values of Nt at $Bi = 0.5$, $M = 5$, $R = 5$, $Le = 10$, $Pr = 10$, $Nb = Nr = 0.5$, $\delta = 0.1$, $\gamma = \lambda = 5$, $\xi = 0.5$.

profiles of velocity in the x-direction, temperature and nanoparticle volume fraction as well as skin friction coefficient, local Nusselt number and local Sherwood number. The key findings of the present investigation are summarized as follows:

1) The increase in slip parameter enhances the velocity profiles, skin friction coefficient and local Nusselt number, while the temperature distributions and local Sherwood number take the inverse behaviors.

2) An improvement in profiles of velocity and temperature can be obtained by increasing the thermophores parameter, while the profiles of nanoparticle volume fraction near the surface, local Nusselt and Sherwood numbers are reduced.

3) The increase in Biot number causes an increase in the hot nanofluid at the surface and consequently the mixed convection is improved.

4) The increase in radiation parameter resists the fluid flow and decreases the fluid temperature.

5) Regardless the values of slip parameter, the increase in Lewis number reduces the fluid velocity and the fluid temperature decreases, gradually, as the Prandtl number increases.

Acknowledgements

The authors extend their appreciation to the editors and reviewers for their comments to improve the quality of the paper.

References

[1] Choi, S.U.S. (1995) Enhancing Thermal Conductivity of Fluids with Nanoparticles. In: *Developments and Applications of Non-Newtonian Flows*, Vol. 231/MD Vol. 66, 99-105.

[2] Buongiorno, J. (2006) Convective Transport in Nanofluids. *Journal of Heat Trans-*

fer, **128**, 240-250. https://doi.org/10.1115/1.2150834

[3] Kuznetsov, A.V. and Nield, D.A. (2010) Natural Convective Boundary-Layer Flow of a Nanofluid Past a Vertical Plate. *International Journal of Thermal Sciences*, **49**, 243-247. https://doi.org/10.1016/j.ijthermalsci.2009.07.015

[4] Schmidt, E. and Beckmann, W. (1930) Das Temperatur-und Geschwindikeitsfeld von einer wärme abgebenden senkrechten Platte bei natürlicher Konvection, II. Die Versuche und ihre Ergibnisse, Forcsh. *Ingenieurwes*, **1**, 391-406. https://doi.org/10.1007/BF02660553

[5] Kuiken, H.K. (1968) An Asymptotic Solution for Large Prandtl Number Free Convection. *Journal of Engineering Mathematics*, **2**, 355-371. https://doi.org/10.1007/BF01579575

[6] Kuiken, H.K. (1969) Free Convection at Low Prandtl Numbers. *Journal of Fluid Mechanics*, **39**, 785e798.

[7] Bejan, A. (1984) Convection Heat Transfer. Wiley, New York.

[8] Kuznetsov, A.V. and Nield, D.A. (2014) Natural Convective Boundary-Layer Flow of a Nanofluid Past a Vertical Plate: A Revised Model. *International Journal of Thermal Sciences*, **77**, 126-129. https://doi.org/10.1016/j.ijthermalsci.2013.10.007

[9] Makinde, O.D. and Aziz, A. (2011) Boundary Layer Flow of a Nanofluid Past a Stretching Sheet with a Convective Boundary Condition. *International Journal of Thermal Sciences*, **50**, 1326-1332. https://doi.org/10.1016/j.ijthermalsci.2011.02.019

[10] Vajravelu, K., Prasad, K.V., Lee, J., Lee, C., Pop, I. and Van Gorder, R.A. (2011) Convective Heat Transfer in the Flow of Viscous Ag-Water and Cu-Water Nanofluids over a Stretching Surface. *International Journal of Thermal Sciences*, **50**, 843-851. https://doi.org/10.1016/j.ijthermalsci.2011.01.008

[11] Ahmed, S.E., Mohamed, S.S., Mansour, M.A. and Mahdy, A. (2016) Heat Transfer and Entropy Generation Due to a Nanofluid over Stretching Cylinder: Effects of Thermal Stratification. *Computational Thermal Sciences*, **9**, 29-47.

[12] Aly, A.M. and Ahmed, S.E. (2016) Double-Diffusive Natural Convective Flow of a Nanofluid over a Vertical Cylinder. *Journal of Nanofluids*, **5**, 110-119.

[13] Makinde, O.D. (2013) Effects of Viscous Dissipation and Newtonian Heating on Boundary-Layer Flow of Nanofluids over a Flat Plate. *International Journal of Numerical Methods for Heat & Fluid Flow*, **23**, 1291-1303. https://doi.org/10.1108/HFF-12-2011-0258

[14] Ahmed, S.E. and Mahdy, A. (2016) Laminar MHD Natural Convection of Nanofluid Containing Gyrotactic Microorganisms over Vertical Wavy Surface Saturated Non-Darcian Porous Media. *Applied Mathematics and Mechanics*, **37**, 471-484.

[15] Takhar, H.S., Chamkha, A.J. and Nath, G. (2001) Unsteady Laminar MHD Flow and Heat Transfer in the Stagnation Region of an Impulsively Spinning and Translating Sphere in the Presence of Buoyancy Forces. *Heat and Mass Transfer*, **37**, 397-402. https://doi.org/10.1007/s002310100227

[16] Chamkha, A.J. and Ahmed, S.E. (2012) Unsteady MHD Heat and Mass Transfer by Mixed Convection Flow in the Forward Stagnation Region of a Rotating Sphere at Different Wall Conditions. *Chemical Engineering Communications*, **199**, 122-141. https://doi.org/10.1080/00986445.2011.575907

[17] Chamkha, A.J. and Ahmed, S.E. (2011) Unsteady MHD Stagnation-Point Flow with Heat and Mass Transfer for a Three-Dimensional Porous Body in the Presence of Heat Generation/Absorption and Chemical Reaction. *Progress in Computational Fluid Dynamics*, **11**, 388-396. https://doi.org/10.1504/PCFD.2011.042848

[18] Chamkha, A.J. and Ahmed, S.E. (2011) Unsteady MHD Heat and Mass Transfer by Mixed Convection Flow in the Forward Stagnation Region of a Rotating Sphere in the Presence of Chemical Reaction and Heat Source. *Proceedings of the World Congress on Engineering*, Vol. 1, London, July 6-8 2011.

[19] Faltas, M.S. and Saad, E.I. (2012) Stokes Flow between Eccentric Rotating Spheres with Slip Regime. *Zeitschrift für Angewandte Mathematik und Physik*, **63**, 905-919. https://doi.org/10.1007/s00033-012-0211-2

[20] Chamkha, A.J. and Ahmed, S.E. (2011) Similarity Solution for Unsteady MHD Flow Near a Stagnation Point of a Three-Dimensional Porous Body with Heat and Mass Transfer, Heat Generation/Absorption and Chemical Reaction. *Journal of Applied Fluid Mechanics*, **4**, 87-94.

[21] Anilkumar, D. and Roy, S. (2004) Self-Similar Solution of the Unsteady Mixed Convection Flow in the Stagnation Point Region of a Rotating Sphere. *Heat and Mass Transfer*, **40**, 487-493. https://doi.org/10.1007/s00033-012-0211-2

[22] Takhar, H.S. and Nath, G. (2000) Self-Similar Solution of the Unsteady Flow in the Stagnation Point Region of a Rotating Sphere with a Magnetic Field. *Heat and Mass Transfer*, **36**, 89-96. https://doi.org/10.1007/s002310050369

[23] Ahmed, S.E. and Mahdy, A. (2016) Unsteady MHD Double Diffusive Convection in the Stagnation Region of an Impulsively Rotating Sphere in the Presence of Thermal Radiation Effect. *Journal of the Taiwan Institute of Chemical Engineers*, **58**, 173-180. https://doi.org/10.1016/j.jtice.2015.06.033

[24] Brewster, M.Q. (1972) Thermal Radiative Transfer Properties. John Wiley and Sons, Hoboken.

Nomenclature

a	Velocity gradient the edge
B	Magnetic field
Bi	Biot number
c_p	Specific heat
D_B	Brownian diffusion coefficient
D_T	Thermophoretic diffusion coefficient
FD	Imensionless stream function
g	Gravity acceleration
Gr_R	Grashof number
h_f	Convective heat transfer coefficient
k	Thermal conductivity of base fluid
k^*	Absorption coefficient
Le	Lewis number
M	Magnetic field parameter
Nr	Buoyancy ratio
Nb	Brownian motion parameter
Nt	Thermophoresis parameter
Nu	Nusselt number
r	Radius of the sphere
R	Radiation parameter
Re_R	Reynolds number
S	Velocity component in-direction y
Sh	Sherwood numbers
t	Time
T	Local fluid temperature
T_f	Temperature of the hot fluid
(u, v, w)	Velocity components in the x, y and z directions
U	Ambient velocity
(x, y, z)	Cartesian coordinates

Greek Symbols

β_T	Coefficient of thermal expansion
μ	Dynamic viscosity
ν	Kinematic viscosity
λ	Rotation parameter
σ	Electrical conductivity
σ_1	Stefan-Boltzman constant
ρ_f	Density of base fluid
ρ_p	Nanoparticle mass density
θ	Dimensionless temperature
ϕ	Dimensionless nanoparticle volume fraction
$(\rho c)_f$	Heat capacity of the base fluid

$(\rho c)_p$	Heat capacity of the nanoparticle material
γ	Buoyancy parameter
δ	Slip parameter
Ω	Angular velocity
(ξ, η)	Non-similarity variables

Subscripts

w	Conditions at the surface
∞	Conditions in the free stream